

# Tuning Optical Properties of Transparent Conducting Barium Stannate by Dimensional Reduction

Yuwei Li<sup>1,2</sup>, Lijun Zhang<sup>3</sup>, Yanming Ma<sup>1</sup>, and David J. Singh<sup>4</sup>

<sup>1</sup>State Key Lab of Superhard Materials, Jilin University, 130012, Changchun, China

<sup>2</sup>Beijing Computational Science Research Center, Beijing 100084, China

<sup>3</sup>College of Materials Science and Engineering, Jilin University, 130012, Changchun, China

<sup>4</sup>Materials Science and Technology Division, Oak Ridge National Laboratory, Oak Ridge, Tennessee 37831-6056

(Dated: March 1, 2022)

We report calculations of the electronic structure and optical properties of doped *n*-type perovskite BaSnO<sub>3</sub> and layered perovskites. While doped BaSnO<sub>3</sub> retains its transparency for energies below the valence to conduction band onset, the doped layered compounds exhibit below band edge optical conductivity due to transitions from the lowest conduction band. This gives absorption in the visible for Ba<sub>2</sub>SnO<sub>4</sub>. Thus it is important to minimize this phase in transparent conducting oxide (TCO) films. Ba<sub>3</sub>Sn<sub>2</sub>O<sub>7</sub> and Ba<sub>4</sub>Sn<sub>3</sub>O<sub>10</sub> have strong transitions only in the red and infrared, respectively. Thus there may be opportunities for using these as wavelength filtering TCO.

Transparent conducting oxides (TCO) are widely used for electrodes in solar energy and display technologies. [1, 2] The most commonly used material is Sn doped In<sub>2</sub>O<sub>3</sub>, known as ITO. This is a stable material that can be readily deposited in thin films and has excellent TCO performance. However, there is interest in alternatives to ITO both because of a desire to reduce the use of In and to identify TCO materials with a range of other properties and functionalities. [3] For displays, high DC conductivity, low haze and high transparency for the operating wavelength and viewing angle ranges are needed. Transparency outside these ranges is not needed and is often undesirable since heating due to infrared transmission and ultraviolet photons can degrade devices, e.g. in outdoor use. We note that transparency below the absorber band gap is undesirable in solar photovoltaic applications. While light filters can be incorporated in various layers of a device architecture, transparent conductors that also act as filters may be useful.

Perovskite structure BaSnO<sub>3</sub> doped by trivalent cation substitutions for Ba (e.g. La) and by Sb alloying on the Sn site shows promise as an ITO alternative. [4–22] Importantly, recent studies of high mobility La doped BaSnO<sub>3</sub> transparent conducting films show transport properties that are still dominated by extrinsic defects, specifically dislocations. [12, 18, 19] The implication is that there remains considerable room for even better conductivity with improvements in film perfection. Recent studies suggested that *n*-type BaSnO<sub>3</sub> may have substantial tunability, e.g. in the band gap via alloying and strain, [14–17] but applications of strain tuning of BaSnO<sub>3</sub> have yet to be demonstrated. Here we show that it is possible to tailor the spectral transmission of BaSnO<sub>3</sub> by a dimensional reduction strategy.

We report first principles calculations for doped BaSnO<sub>3</sub>, in relation to members of the Ruddlesden-Popper homologous series derived from BaSnO<sub>3</sub> by periodic insertion of nominally insulating BaO layers. The first two members of the series are known bulk equilibrium stable phases in the BaO – SnO<sub>2</sub> pseudobinary phase diagram that are readily made using com-

mon methods. [23–29] Perhaps other phases can also be grown, in analogy with the Sr-Ti-O system. [30] This is also consistent with the Sr-Sn-O system, which has a known Ruddlesden-Popper series. [31, 32] Kamimura and co-workers have recently shown that members of the Sr-Sn-O Ruddlesden-Popper series can show very different luminescence properties when activated. [33] Furthermore, the members of the Ba-Sn-O Ruddlesden-Popper series have good in plane lattice matches with each other and are presumably compatible with each other in thin film form.

The experimental lattice parameters and spacegroups are BaSnO<sub>3</sub>, cubic, *Pm3m*  $a=4.116$  Å, [34–36] Ba<sub>2</sub>SnO<sub>4</sub>, body centered tetragonal, *I4/mmm*,  $a=4.1411$  Å,  $c=13.2834$  Å, [25] and Ba<sub>3</sub>Sn<sub>2</sub>O<sub>7</sub>, body centered tetragonal, *I4/mmm*,  $a=4.129$  Å,  $c=21.460$  Å. [24] As discussed below, we also did calculations for the next member of the series, Ba<sub>4</sub>Sn<sub>3</sub>O<sub>10</sub>, which is a phase that has not been reported experimentally. For this we did calculations both using a fully relaxed structure and a partially relaxed structure in which the atomic coordinates were relaxed but the lattice parameters were fixed to interpolated experimental values from the known phases.

The main first principles calculations were performed using the general potential linearized augmented planewave (LAPW) method [37] as implemented in the WIEN2k code. We also did calculations to cross-check using the VASP code with hybrid HSE06 functional [38, 39] and the generalized gradient approximation of Perdew, Burke and Ernzerhof (PBE-GGA). [40]

For the LAPW calculations, we used well converged basis sets including local orbitals for the semicore states of the alkaline earth elements, the O *2p* state and the Sn *4d* state. We used the standard LAPW basis sets rather than the APW+lo method. [41] The LAPW sphere radii were 2.4 bohr, 2.25 bohr and 1.6 bohr for Ba, Sn and O, respectively, and a basis set cut-off,  $k_{max}$ , set by the criterion  $R_{min}k_{max}=7.0$  was used, where  $R_{min}$  is the O LAPW sphere radius.

We fixed the lattice parameters to the experimental values and relaxed the internal atomic coordinates of the

layered compounds using the PBE-GGA. Following the structure optimization, we did electronic structure and optical calculations using the modified Becke-Johnson type potential functional of Tran and Blaha, [42] denoted TB-mBJ in the following. This potential gives band gaps in remarkably good accord with experiment for a wide variety of simple semiconductors and insulators, [42–46] including perovskite stannates. [15] We compared the TB-mBJ results for the undoped compounds with HSE06 calculations as discussed below.

Doping by La was treated using the virtual crystal approximation. The virtual crystal approximation is an average potential approximation. It goes beyond rigid bands, and specifically includes composition dependent distortions of the band structure. The use of the virtual crystal approximation is supported by the fact that in these compounds the highly electropositive elements, Ba and La, are fully ionized and serve only to stabilize the structure and donate charge to the conducting bands derived from Sn and O. Ba<sub>3</sub>Sn<sub>2</sub>O<sub>7</sub> has two crystallographically distinct Ba sites, *i.e.* the *2b* perovskite-like site between the two SnO<sub>2</sub> layers and the *4e* rocksalt-like site in between the perovskite blocks (Fig. 1). For this compound we performed calculations in which we did virtual crystal with La on site *2b*, on site *4e* and equally distributed on the two sites. The results were practically the same, which supports the validity of the virtual crystal approximation.

There have been a number of prior first principles studies of BaSnO<sub>3</sub> as well as the related perovskites, CaSnO<sub>3</sub> and SrSnO<sub>3</sub>. The Sn *s* nature of the conduction band and its role in the good conductivity of *n*-type doped BaSnO<sub>3</sub> were established early on. [5] This basic result was found in subsequent band structure calculations with various methods. [12–22] Large variation in the band gap between BaSnO<sub>3</sub>, SrSnO<sub>3</sub> and CaSnO<sub>3</sub>, was found by Mizoguchi and co-workers [13], and subsequently discussed in terms of strain. [15, 17]

The band structures with the TB-mBJ potential are shown in Fig. 2. The calculated indirect gaps using the TB-mBJ potential are 2.82 eV, 4.22 eV and 3.53 eV for BaSnO<sub>3</sub>, Ba<sub>2</sub>SnO<sub>4</sub> and Ba<sub>3</sub>Sn<sub>2</sub>O<sub>7</sub>, respectively. The calculated TB-mBJ band gap of bulk NaCl structure BaO, lattice parameter 5.523 Å, is 3.61 eV, indirect between *X* and  $\Gamma$ . Two aspects that are immediately apparent from the band structures are (1) the layered compounds show a dispersive *s* band at the conduction band minimum similar to BaSnO<sub>3</sub> and (2) the layered compounds show little dispersion in the *c*-axis direction, so the layering is indeed strongly reflected in the electronic structure. The band narrowing in the *c*-axis direction is a kind of quantum confinement effect.

Table I gives the band gaps as obtained with the PBE-GGA functional, the TB-mBJ potential and the HSE06 hybrid functional. As may be seen there is a good agreement between the TB-mBJ and the HSE06 results, while as usual the PBE-GGA underestimates gaps.

Fig. 3 gives the in-plane plasma frequencies,  $\Omega_p$  for

TABLE I. Band gaps for the Ba-Sn-O Ruddlesden-Popper compounds as obtained with the PBE-GGA functional, the TB-mBJ potential and the HSE06 hybrid functional.

Compound	PBE-GGA (eV)	TB-mBJ (eV)	HSE06 (eV)
BaSnO <sub>3</sub>	0.98	2.82	2.66
Ba <sub>4</sub> Sn <sub>3</sub> O <sub>10</sub>	1.61	3.24	3.21
Ba <sub>3</sub> Sn <sub>2</sub> O <sub>7</sub>	2.03	3.53	3.60
Ba <sub>2</sub> SnO <sub>4</sub>	2.83	4.22	4.41

*n*-type doping as a function of doping in carriers per Sn. Conductivity in metals and degenerately doped semiconductors depends on the plasma frequency,  $\sigma \propto \Omega_p^2 \tau$  where  $\tau$  is an effective inverse scattering rate. As seen, if one assumes similar scattering rates, the conductivity follows a perhaps expected trend following the density of Sn ions (*i.e.* falling as the concentration of insulating BaO increases). Specifically, for in-plane conduction,  $\sigma(\text{BaSnO}_3) > \sigma(\text{Ba}_3\text{Sn}_2\text{O}_7) > \sigma(\text{Ba}_2\text{SnO}_4)$ . The volumes per Sn are 69.73 Å<sup>3</sup>, 91.47 Å<sup>3</sup> and 113.90 Å<sup>3</sup>, for BaSnO<sub>3</sub>, Ba<sub>3</sub>Sn<sub>2</sub>O<sub>7</sub> and Ba<sub>2</sub>SnO<sub>4</sub>, respectively. The BaO layers, while not contributing to conduction, also would not be expected to contribute to optical absorption, and therefore the result suggests that the layered compounds could be good TCO as well. As discussed below, our optical calculations show that this may be the case for Ba<sub>3</sub>Sn<sub>2</sub>O<sub>7</sub> and higher members of the series, but is not the case for Ba<sub>2</sub>SnO<sub>4</sub>.

The good TCO behavior of BaSnO<sub>3</sub> can be understood in terms of three main reasons: (1) The material can be effectively doped *n*-type to high carrier concentrations, (2) It has a highly dispersive Sn *s* derived conduction band that leads to high mobility and (3) there is a large gap between the lowest conduction band at the conduction band minimum (CBM), which is at  $\Gamma$ , and the next conduction band at  $\Gamma$ .

The calculated absorption spectra for virtual crystal doped BaSnO<sub>3</sub> are shown in Fig. 4. As seen, the optical gap increases with carrier concentration. This is a consequence both of the electrostatic effect of adding electrons to a band (electrons added to the Sn *s* derived conduction band by doping provide a repulsion to other electrons in this orbital raising the energy of the band), and the increase in Fermi level within the band as electrons are added. Here the Fermi level shift is the larger effect. For example, with 0.2 electrons per Sn, we obtain a Fermi level 1.99 eV above the conduction band minimum in our virtual crystal calculations, while the indirect gap between the valence band maximum and conduction band minimum increases by only 0.14 eV. This latter increase is a non-rigid-band effect. In addition to this band gap there are other small distortions of the band structure. This is shown in Fig. 5.

The increase in apparent optical gap with La doping is possibly consistent with optical absorption spectra of BaSnO<sub>3</sub> and (Ba,La)SnO<sub>3</sub> obtained by Kim and co-workers, [12] whose experimental spectra show such

an increase. However, in view of the broadening of the reported experimental spectra with La addition further measurements would be desirable.

The band structures of  $\text{Ba}_2\text{SnO}_4$  and  $\text{Ba}_3\text{Sn}_2\text{O}_7$  do not show large gaps above the CBM, but instead show other bands within 3 eV of the CBM. These arise from the dimensional reduction, specifically the strongly reduced hopping along the  $k_z$ ,  $c$ -axis direction, which narrows the conduction bands. Additionally, in  $\text{Ba}_3\text{Sn}_2\text{O}_7$ , there are two perovskite layers in the perovskite block, which leads to a band structure with pairs of bands in the  $k_z=0$  plane that are characterized by even or odd symmetry with respect to reflection in the BaO plane between the  $\text{SnO}_2$  layers. Such pairs of bands are then strongly connected by dipole transitions for electric field polarization along the  $c$ -axis direction, but not for in-plane polarization, *i.e.* not for light propagating along the  $c$ -axis direction.

Other consequences of the dimensional reduction are a higher density of states near the CBM corresponding to the near 2D electronic structure (note the flatness of the lowest band along the  $Z$ - $\Gamma$  direction); a 2D electronic structure has a high, constant density of states near the band edge, while a 3D band structure has a lower initial density of states,  $N(E) \propto E^{1/2}$ , with  $E$  relative to the CBM. This is clearly seen in the densities of states (DOS), shown for the conduction bands in Fig. 6. In particular, the DOS for  $\text{BaSnO}_3$  shows a smooth increase with energy, while prominent steps corresponding to band onsets are present for the layered compounds. The consequence of this stepped DOS is that in 2D the doping dependence of the Fermi level,  $E_F$ , will be weaker, with the result that higher doping levels might be possible, and that following arguments given elsewhere the thermopower will be strongly enhanced. [47, 48] For the conductivity,  $\sigma$  in plane is generically expected to remain similar to the 3D compound at the expense of a very strong reduction in  $c$ -axis conductivity. This means that use of  $\text{Ba}_2\text{SnO}_4$  or  $\text{Ba}_3\text{Sn}_2\text{O}_7$  films as conducting oxides would require the production of textured films.

The optical conductivities of the doped compounds are given in Fig. 7, showing both in-plane and out-of-plane directions. These plots include a Drude contribution, with the Drude weight from the calculated  $\Omega_p$  and an assumed broadening,  $\gamma=0.1$ . Although undoped  $\text{Ba}_2\text{SnO}_4$  is the compound with the highest band gap, it shows strong optical conductivity (and absorption) in the visible for light polarization in the  $c$ -axis direction, but low optical conductivity for polarization in the plane, which is the case for normal incidence. This might suggest that  $\text{Ba}_2\text{SnO}_4$  could be used as a transparent conductor for normal incident light. This may, however, be misleading, since in reality the disorder would lead to symmetry breaking, which could then result in some absorption for normal incident light as well. In any case, this absorption is a consequence of interband transitions from the lowest conduction band to higher bands near the zone center.

$\text{Ba}_3\text{Sn}_2\text{O}_7$  shows different behavior. It displays very strong interband transitions for  $c$ -axis polarized light in

the infrared and red (below  $\sim 2$  eV). These lead to high peaks in the optical conductivity for  $c$ -axis polarization even at moderate doping. This polarization involves dipole transitions between bands with opposite reflection symmetry in the plane between the  $\text{SnO}_2$  layers as mentioned above. The band making up the CBM has even reflection symmetry, with an onset of odd reflection symmetry states 1.7 eV above the CBM. Importantly,  $\text{Ba}_3\text{Sn}_2\text{O}_7$  does not show significant absorption in the visible above 2 eV for either light polarization, but would be expected to be strongly absorbing below 2 eV for electric field out of plane and in the presence of disorder for both polarizations. More generally, the insertion of BaO layers into  $\text{BaSnO}_3$  breaks the translational symmetry along the  $c$ -axis direction. This then allows dipole transitions for electric field polarization along the  $c$ -axis since the bands folded back to  $\Gamma$  are from different original crystal momenta along  $k_z$  (note that the dipole operator is equivalent to a momentum operator).

As mentioned, we also did calculations for hypothetical  $\text{Ba}_4\text{Sn}_3\text{O}_{10}$ , which is the next member of the homologous series. For this, we used lattice parameters based on interpolation using the experimental lattice parameters of  $\text{BaSnO}_3$ ,  $\text{Ba}_4\text{SnO}_4$  and  $\text{Ba}_3\text{Sn}_2\text{O}_7$ . We then fully relaxed the internal atomic coordinates within this cell. The lattice parameters used were from interpolation,  $a=4.125$  Å, and  $c=29.637$  Å. Full relaxation with the PBE-GGA yielded slightly larger lattice parameters of  $a=4.202$  Å, and  $c=30.170$  Å, also with relaxation of the internal atomic coordinates. The calculated band gaps are 3.24 eV for the interpolated structure and 2.64 eV for the larger volume cell with fully relaxed lattice parameters. The band structure for the interpolated lattice parameters is shown in Fig. 2. The in-plane plasma frequency and density of states and optical conductivities are shown along with those of the other compounds. As seen, its properties generally interpolate between those of  $\text{BaSnO}_3$  and  $\text{Ba}_3\text{Sn}_2\text{O}_7$ .

We calculated the energetics of the known compounds, along with those of hypothetical compounds based on addition of an extra BaO layer between the perovskite blocks in the series, *i.e.*  $\text{Ba}_5\text{Sn}_3\text{O}_{11}$ , and the next member of the series,  $\text{Ba}_5\text{Sn}_4\text{O}_{13}$ . The resulting convex hull for the BaO- $\text{SnO}_2$  pseudobinary is shown in Fig. 8. These calculations were done using the PBE-GGA with fully relaxed structures, to get a consistent set of energies. As seen, there is a strong tendency towards compound formation in this pseudobinary. The stable compounds are  $\text{BaSnO}_3$ ,  $\text{Ba}_2\text{SnO}_4$  and  $\text{Ba}_3\text{Sn}_2\text{O}_7$ . The other compounds are above the convex hull, meaning that they are not predicted to be ground state phases in this pseudobinary. However, they are very close to the hull, within 0.02 eV/atom ( $\sim 240$  K). This is certainly below the uncertainty of our density functional calculations. Therefore what can be concluded is that these phases are either on or slightly above the convex hull. Based on these results it is likely that they can be stabilized in thin films where kinetic constraints may prevent phase separation,

[49] and perhaps also under other conditions.

Experimental results have shown that heavily  $n$ -type doped  $\text{BaSnO}_3$  is promising as a high performance TCO with good conductivity and optical transparency in the visible. Layered perovskite variants of this material can be readily made, and it is likely that they can be layered with the cubic perovskite material based on the similar chemistry and in-plane lattice parameter.

In fact, it may well be that conventionally made films incorporate some fraction of these phases. The present calculations show that these phases would not necessarily be harmful for the DC conductivity especially if a high degree of texture is present. However, we find that the presence of doped  $\text{Ba}_2\text{SnO}_4$  would be harmful to the visible light transparency. It is possible in fact that some of the variable results seen in experiments are due to the presence of different amounts of  $\text{Ba}_2\text{SnO}_4$  related to various amounts of Sn deficiency. It would be desirable to minimize the occurrence of this phase to im-

prove the transparency. On the other hand, the occurrence of bi-layer  $\text{Ba}_3\text{Sn}_2\text{O}_7$  and higher members of the series such as  $\text{Ba}_4\text{Sn}_3\text{O}_{10}$  may not be detrimental and may add useful functionality, such as energy selective filtering. We note that a related concept was recently developed and exploited to produce low loss, room temperature tunable dielectrics based on  $\text{SrTiO}_3$ , specifically using the  $\text{Sr}_{n+1}\text{Ti}_n\text{O}_{3n+1}$  Ruddlesden-Popper phases with  $n \geq 3$ . [30] The present results indicate that it will be interesting to experimentally explore the incorporation of Ruddlesden-Popper phases into  $n$ -type Ba-Sn-O TCO films as a functional tuning parameter.

YL and YM acknowledge funding support from the Natural Science Foundation of China (Grant No. 11025418). LZ acknowledges funding from the Recruitment Program of Global Experts (the Thousand Young Talents Plan). Work at ORNL was supported by the Department of Energy, Office of Science, Basic Energy Sciences, Materials Sciences and Engineering Division.

- 
- [1] D. S. Ginley and C. Bright, *MRS Bull.* **25**, 15 (2000).  
 [2] H. Kawazoe, H. Yanagi, K. Ueda, and H. Hosono, *MRS Bull.* **25**, 28 (2000).  
 [3] T. Minami, *Thin Solid Films* **516**, 5822 (2008).  
 [4] R. J. Cava, P. Gammel, B. Batlogg, J. J. Krajewski, and W. F. Peck, Jr., *Phys. Rev. B* **42**, 4815 (1990).  
 [5] D. J. Singh, D. A. Papaconstantopoulos, J. P. Julien, and F. Cyrot-Lackmann, *Phys. Rev. B* **44**, 9519 (1991).  
 [6] S. Upadhyay, O. Parkash, and D. Kumar, *J. Phys. D: Appl. Phys.* **37**, 1483 (2004).  
 [7] B. Hadjarab, A. Bouguelia, and M. Trari, *J. Phys. D: Appl. Phys.* **40**, 5833 (2007).  
 [8] H. F. Wang, Q. Z. Liu, F. Chen, G. Y. Gao, W. Wu, and X. H. Chen, *J. Appl. Phys.* **101**, 106105 (2007).  
 [9] H. J. Kim, U. Kim, H. M. Kim, T. H. Kim, H. S. Mun, B. G. Jeon, K. T. Hong, W. J. Lee, C. Ju, K. H. Kim, and K. Char, *Appl. Phys. Express* **5**, 061102 (2012).  
 [10] X. Luo, Y. S. Oh, A. Sirenko, P. Gao, T. A. Tyson, K. Char, and S. W. Cheong, *Appl. Phys. Lett.* **100**, 172112 (2012).  
 [11] Q. Liu, J. Liu, B. Li, H. Li, G. Zhu, K. Dai, Z. Liu, P. Zhang, and J. Dai, *Appl. Phys. Lett.* **101**, 241901 (2012).  
 [12] H. J. Kim, U. Kim, T. H. Kim, J. Kim, H. M. Kim, B.-G. Jeon, W.-J. Lee, H. S. Mun, K. T. Hong, J. Yu, K. Char, and K. H. Kim, *Phys. Rev. B* **86**, 165205 (2012).  
 [13] H. Mizoguchi, H. W. Eng, and P. M. Woodward, *Inorg. Chem.* **43**, 1667 (2004).  
 [14] H. Mizoguchi, P. Chen, P. Boolchand, V. Ksenofontov, C. Felser, P. W. Barnes, and P. M. Woodward, *Chem. Mater.* **25**, 3858 (2013).  
 [15] X. F. Fan, W. T. Zheng, X. Chen, and D. J. Singh, *PLoS One* **9**, e91423 (2014).  
 [16] H. R. Liu, J. H. Yang, H. J. Xiang, and S. H. Wei, *Appl. Phys. Lett.* **102**, 112109 (2013).  
 [17] D. J. Singh, Q. Xu, and K. P. Ong, *Appl. Phys. Lett.* **104**, 011910 (2014).  
 [18] H. Mun, U. Kim, H. M. Kim, C. Park, T. H. Kim, H. J. Kim, K. H. Kim, and K. Char, *Appl. Phys. Lett.* **102**, 252105 (2013).  
 [19] P. V. Wadekar, J. Alaria, M. O'Sullivan, N. L. O. Flack, T. D. Manning, L. J. Phillips, K. Durose, O. Lozano, S. Lucas, J. B. Claridge, and M. J. Rosseinsky, *Appl. Phys. Lett.* **105**, 052104 (2014).  
 [20] S. Sallis, D. O. Scanlon, S. C. Chae, N. F. Quackenbush, D. A. Fischer, J. C. Woicik, J. H. Guo, S. W. Cheong, and L. F. J. Piper, *Appl. Phys. Lett.* **103**, 042105 (2013).  
 [21] D. O. Scanlon, *Phys. Rev. B* **87**, 161201 (2013).  
 [22] B. G. Kim, J. Y. Jo, and S. W. Cheong, *J. Solid State Chem.* **197**, 134 (2013).  
 [23] G. Wagner and H. Binder, *Z. Anorg. Allg. Chem.* **298**, 12 (1959).  
 [24] Y. Hinatsu and K. Tezuka, *J. Solid State Chem.* **138**, 329 (1998).  
 [25] M. A. Green, K. Prassides, P. Day, and D. A. Neumann, *J. Chem. Soc., Faraday Trans.* **92**, 2155 (1996).  
 [26] B. J. Kennedy, *Aust. J. Chem.* **50**, 917 (1997).  
 [27] R. C. Ropp, *Encyclopedia of the Alkaline Earth Compounds* (Elsevier, Amsterdam, 2012) p. 454.  
 [28] T. Yamashita and K. Ueda, *J. Solid State Chem.* **180**, 1410 (2007).  
 [29] A. Stanulis, S. Sakirzanovas, M. Van Bael, and A. Kareiva, *J. Sol-Gel Sci. Technol.* **64**, 643 (2012).  
 [30] C. H. Lee, N. D. Orloff, T. Biroi, Y. Zhu, V. Goian, E. Rocas, R. Haislmaier, E. Vlahos, J. A. Mundy, L. F. Kourkoutis, Y. Nie, M. D. Biegalski, J. Zhang, M. Bernhagen, N. A. Benedek, Y. Kim, J. D. Brock, R. Uecker, X. X. Xi, V. Gopalan, D. Nuzhnyy, S. Kamba, D. A. Muller, I. Takeuchi, J. C. Booth, C. J. Fennie, and D. G. Schlom, *Nature (London)* **502**, 532 (2013).  
 [31] M. A. Green, K. Prassides, P. Day, and D. A. Neumann, *Int. J. Inorg. Mater.* **2**, 35 (2000).  
 [32] W. T. Fu, D. Visser, K. S. Knight, and D. J. W. Ijdo, *J. Solid State Chem.* **177**, 4081 (2004).  
 [33] S. Kamimura, H. Yamada, and C. N. Xu, *Appl. Phys. Lett.* **101**, 091113 (2012).  
 [34] A. Vegas, M. Vallet-Regi, J. M. Gonzalez-Calbet, and M. A. Alario-Franco, *Acta Cryst. B* **42**, 167 (1986).

- [35] T. Maekawa, K. Kurosaki, and S. Yamanaka, *J. Alloys Compds.* **416**, 214 (2006).
- [36] E. Bevilion, A. Chesnaud, Y. Wang, G. Dezanneau, and G. Geneste, *J. Phys.:Condens. Matter* **20**, 145217 (2008).
- [37] D. J. Singh and L. Nordstrom, *Planewaves Pseudopotentials and the LAPW Method, 2nd Edition* (Springer, Berlin, 2006).
- [38] J. Heyd, G. E. Scuseria, and M. Ernzerhof, *J. Chem. Phys.* **118**, 8207 (2003).
- [39] J. Heyd, G. E. Scuseria, and M. Ernzerhof, *J. Chem. Phys.* **124**, 219906 (2006).
- [40] J. P. Perdew, K. Burke, and M. Ernzerhof, *Phys. Rev. Lett.* **77**, 3865 (1996).
- [41] E. Sjostedt, L. Nordstrom, and D. J. Singh, *Solid State Commun.* **114**, 15 (2000).
- [42] F. Tran and P. Blaha, *Phys. Rev. Lett.* **102**, 226401 (2009).
- [43] D. Koller, F. Tran, and P. Blaha, *Phys. Rev. B* **83**, 195134 (2011).
- [44] D. J. Singh, *Phys. Rev. B* **82**, 155145 (2010).
- [45] Y. S. Kim, M. Marsman, G. Kresse, F. Tran, and P. Blaha, *Phys. Rev. B* **82**, 205212 (2010).
- [46] D. J. Singh, *Phys. Rev. B* **82**, 205102 (2010).
- [47] L. D. Hicks and M. S. Dresselhaus, *Phys. Rev. B* **47**, 12727 (1993).
- [48] X. Chen, D. Parker, and D. J. Singh, *Sci. Rep.* **3**, 3168 (2013).
- [49] M. D. Hornbostel, E. J. Hyer, J. Thiel, and D. C. Johnson, *J. Am. Chem. Soc.* **119**, 2665 (1997).

## FIGURE CAPTIONS

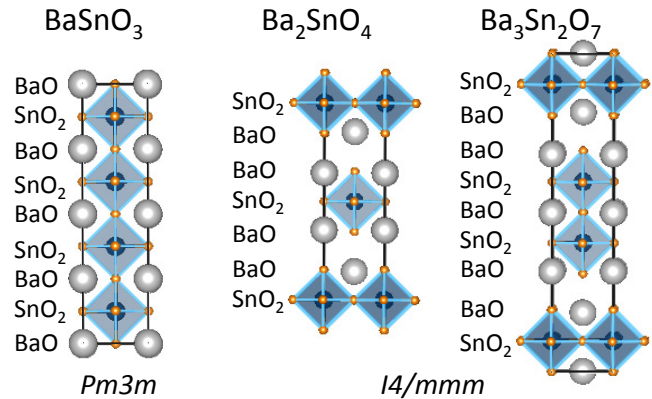


FIG. 1. Cubic perovskite structure and the first two members of the Ruddlesden-Popper series, showing the stacking of BaO and SnO<sub>2</sub> layers.

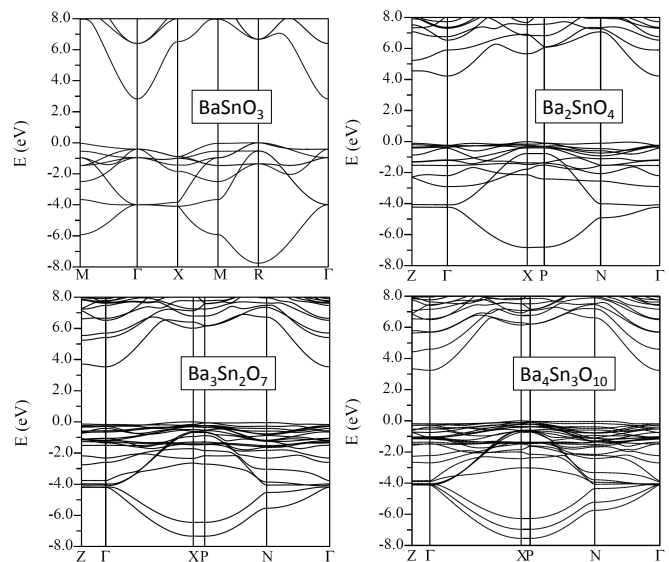


FIG. 2. Band structures of cubic BaSnO<sub>3</sub>, and body centered tetragonal Ba<sub>2</sub>SnO<sub>4</sub>, Ba<sub>3</sub>Sn<sub>2</sub>O<sub>7</sub> and hypothetical Ba<sub>4</sub>Sn<sub>3</sub>O<sub>10</sub>. The band structure of BaSnO<sub>3</sub> is that previously reported in Ref. 15, reproduced with permission from PLoS ONE **9**, e91423 (2014). Copyright 2014 Fan, Zheng, Chen and Singh, an open access work distributed under the terms of the Creative Commons Attribution License.

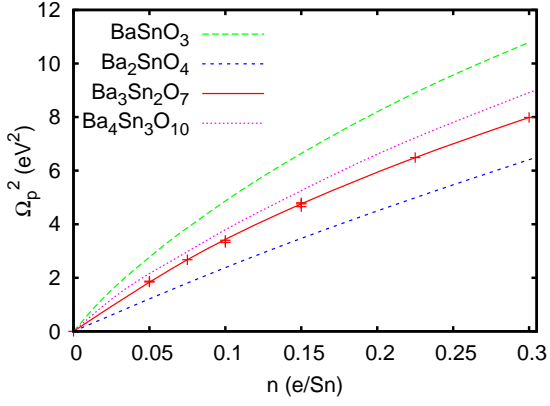


FIG. 3. In-plane square plasma frequency of  $n$ -type  $\text{BaSnO}_3$ ,  $\text{Ba}_2\text{SnO}_4$ ,  $\text{Ba}_3\text{Sn}_2\text{O}_7$  and hypothetical  $\text{Ba}_4\text{Sn}_3\text{O}_{10}$  as a function of carrier concentration in electrons per Sn atom. Calculations were done for doping on the different Ba-sites in  $\text{Ba}_3\text{Sn}_2\text{O}_7$  (see text) with data indicated by points.

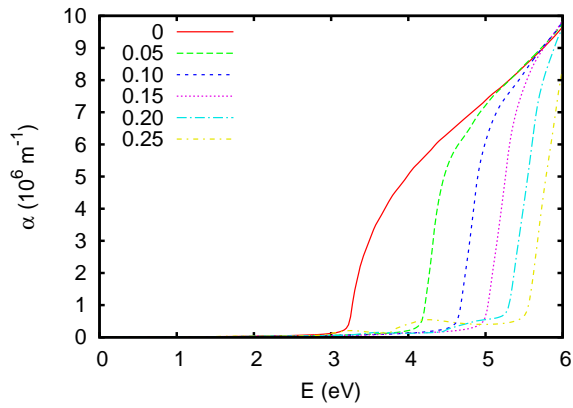


FIG. 4. Calculated absorption spectra for  $n$ -type  $\text{BaSnO}_3$  as a function of doping level in carriers per Sn. The data for zero doping are from Ref. 15.

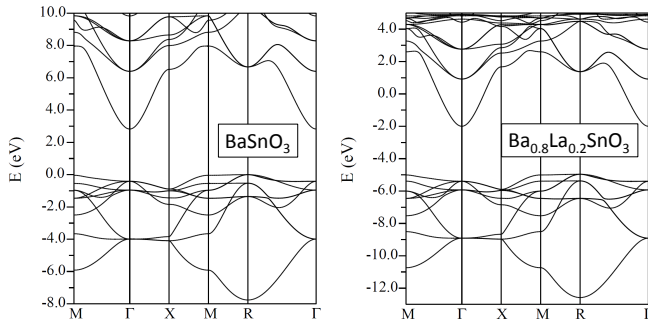


FIG. 5. Comparison of the band structure of undoped  $\text{BaSnO}_3$  (left) and virtual crystal  $\text{Ba}_{0.8}\text{La}_{0.2}\text{SnO}_3$  (right). The energy zero is at the valence band maximum for  $\text{BaSnO}_3$  and at the Fermi level for the doped compound. Note the relatively minor band distortions.

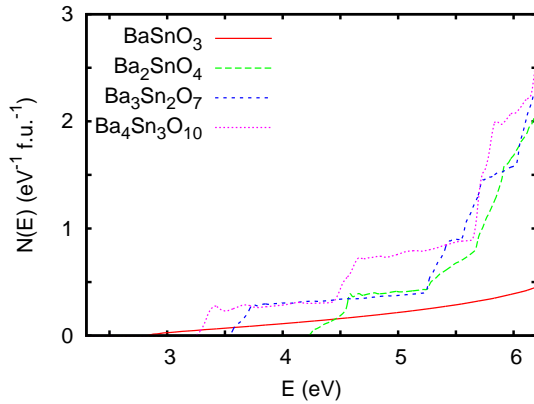


FIG. 6. Calculated electronic DOS for the conduction bands. The energy zero is at the valence band maximum. Note the step like features for all of the layered compounds.

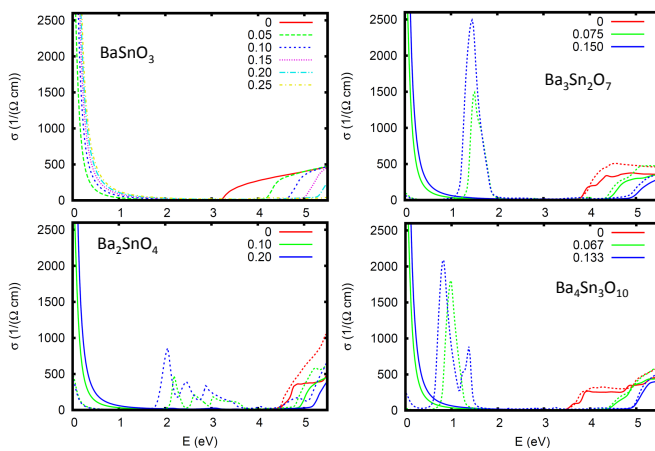


FIG. 7. Optical conductivities of  $\text{BaSnO}_3$ ,  $\text{Ba}_2\text{SnO}_4$ ,  $\text{Ba}_3\text{Sn}_2\text{O}_7$  and hypothetical  $\text{Ba}_4\text{Sn}_3\text{O}_{10}$  at various doping levels in units of electrons per Sn. For the layered compounds, the solid lines are for the in-plane,  $a$ -axis conductivities, while the dashed lines are for the  $c$ -axis conductivities.

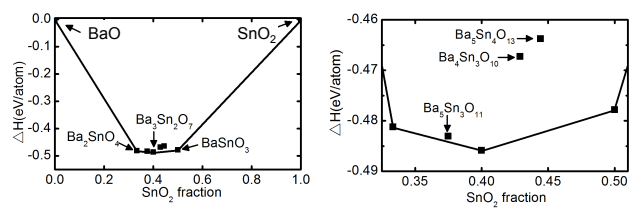


FIG. 8. Convex hull for the pseudobinary system BaO–SnO<sub>2</sub>. The full composition range, with the stable compounds indicated is in the left panel. The right panel shows an expanded view of the region studied, with the compounds above the hull indicated.